



# Characterization of El Kherba landslide triggered by the August 07, 2020, $M_w = 4.9$ Mila earthquake (Algeria) based on post-event field observations and ambient noise analysis

Mohamed Yacine Tebbouche<sup>1,2,3</sup> · Dalila Ait Benamar<sup>1</sup> · Hany. M. Hassan<sup>4</sup> · A. P. Singh<sup>5</sup> · Raouf Bencharif<sup>1</sup> · Djamel Machane<sup>1</sup> · Abdelghani Aghiles Meziani<sup>1</sup> · Zoubida Nemer<sup>2</sup>

Received: 3 March 2021 / Accepted: 2 January 2022 / Published online: 17 January 2022  
© The Author(s), under exclusive licence to Springer-Verlag GmbH Germany, part of Springer Nature 2022

## Abstract

On 7th of August 2020, a  $M_w = 4.9$  earthquake occurred in Mila province (Northeast Algeria). Consequently, more than 2000 houses were indirectly affected (partially damaged or collapsed) within 10 km from the earthquake's epicenter, in the locality of El Kherba. According to field surveys conducted 3 days after the earthquake, damages and casualties were directly linked to an earthquake-induced landslide that occurred after the main shock. This was evidenced by numerous cracks in the site's soil mainly perpendicular to the landslide direction. Local characteristics (i.e., geology, geomorphology) and anthropogenic activities expose this area to landslide hazard. This study shows the reliability of the ambient noise horizontal to vertical spectral ratio (HVSr) method in the characterization of an active landslide. Ambient noise records were processed through spectral ratio techniques to identify the landslide's geometry based on spectral responses analysis. The obtained results allowed the landslide's slip surface mapping and boundary delineation, which correlates well with the field observations. After the rotation of the signal's horizontal components, large variations in the experimental spectral ratios, in both amplitude and direction, revealed site effects (soil remoulding, crack network) on the soil dynamic behavior.

**Keywords** Earthquake-induced landslide · Horizontal-to-vertical spectral ratio (HVSr) method · Site effects · Landslide hazard · Northeast Algeria

## Introduction

On August 7, 2020, shallow moderate earthquake of  $M_w = 4.9$  and 19 km focal depth occurred in Mila province in the Eastern Tellian Atlas of Algeria (Fig. 1). Two hours after the origin time of the earthquake, an earthquake-induced landslide occurred in El Kherba city at about 10.76 km from the epicenter (Fig. 1). The area was not recognized as a landslide prone area prior to that date. Subsequently, the landslide resulted in severe ground deformations, as well as damages to buildings (i.e., collapse and tilting) roads and sidewalks (i.e., deformation and subsidence), and important infrastructures. As a result, more than 750 families were affected and displaced.

The available earthquake catalogs indicate that many earthquakes of similar magnitude have occurred in Northern Algeria (Harbi et al. 1999; Benfedda et al. 2020). The October 27, 1985 earthquake of  $M_s = 5.9$  in the Eastern Tellian Atlas was the largest instrumentally recorded in the region (Ousadou et al. 2013). Harbi et al. (2003) have clearly

✉ Mohamed Yacine Tebbouche  
ytebbouche@usthb.dz

<sup>1</sup> CGS, Centre National de Recherche Appliquée en Génie Parasismique, Rue Kaddour Rahim, Hussein Dey, 16040 Algiers, Algeria

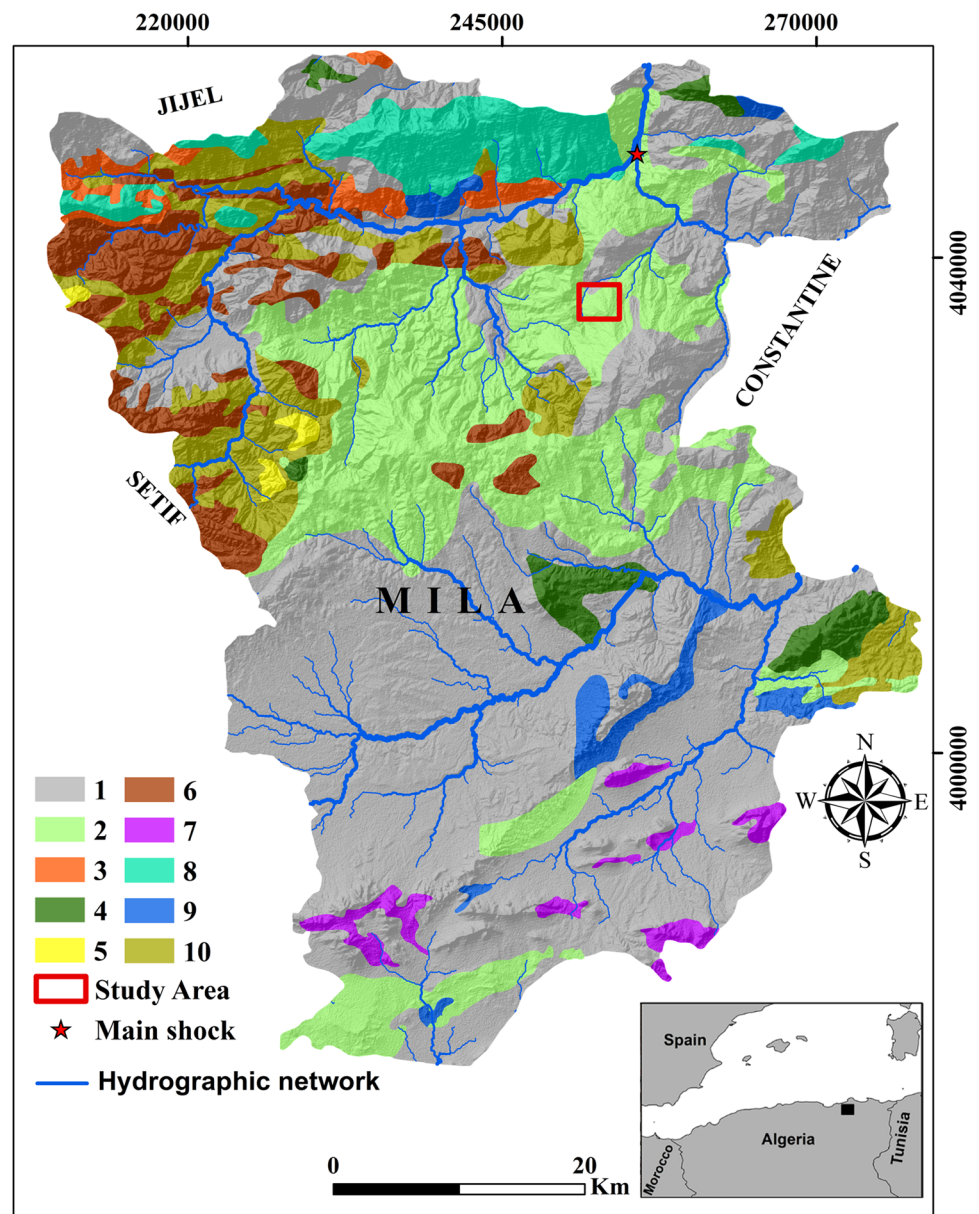
<sup>2</sup> Laboratoire de Géophysique, (FSTGAT), Université des Sciences et de la Technologie Houari Boumediene (USTHB), Bab Ezzouare, Algiers, Algeria

<sup>3</sup> Département des Sciences de la Terre, Institut d'Architecture et des Sciences de la Terre (IAST), Université Ferhat Abbas, Sétif 1 (UFAS1), Campus El Bez, 19000 Sétif, Algeria

<sup>4</sup> Egyptian National Data Center, National Research Institute of Astronomy and Geophysics, Helwan 11421, Egypt

<sup>5</sup> National Centre for Seismology, Ministry of Earth Sciences, Lodhi Road, New Delhi 110003, India

**Fig. 1** Geo-lithologic map of Mila province. The red square represents the study area where El Kherba village is located. The red star marks the main shock located 10.76 km from the study area. 1: alluvium, 2: clay, 3: kaolin clays, 4: limestone, 5: marly limestone, 6: flint limestone, 7: dolomites, 8: sandstone, 9: gypsum, 10: marl



reported that this region is characterized by low-to-moderate seismicity ( $M_s < 6.3$ ) as a result of the ongoing compressional tectonic setting caused by the African-Eurasian plate convergence (Yelles-Chaouche et al. 2006). It is worth mentioning that, based on available earthquake catalogs, prior to the occurrence of August 7, 2020, Mila region had never experienced a locally generated earthquake of tectonic origin. However, thousands of microearthquakes, that are recognized as induced seismicity (Semmane et al. 2012) due to human activity (water pumping), have been reported.

Several studies have investigated the landslide phenomenon worldwide (e.g., Sato and Harp 2009; Sassa et al. 1996; Chousianitis et al. 2014; Martino et al. 2019; Delgado et al. 2011). Due to the fact that landslides can occur as a result

of predisposing and triggering factors (e.g., regional geomorphological, gravitational, geotechnical, climatic, geological and seismotectonic conditions), several regions in northern Algeria are defined and recognized as landslide prone areas (Ogila et al. 2021). For instance, the most well-known landslides triggered by an earthquake are: Kherata landslide in 1949 (Gabert 1984), Boumerdes landslide (May 21, 2003) (Machane et al. 2004), Lâalam landslide on March 20, 2006 (Guemache et al. 2010), and the most recent landslide of August 7, 2020 in Mila province. In this area, few studies have focused on the major development challenge that local ground instabilities present. However, Marmi et al. (2008) highlighted that the landslide hazard presents a major threat to this region's inhabitants, buildings,

and other infrastructures. Moreover, Merghadi et al. (2018) compared machine-learning methods and demonstrated their effectiveness in landslide susceptibility assessment in Mila region. Globally, one pioneer piece of work in this field is Keefer (1984), where 40 historical landslides were studied, characterized, and correlated with earthquake magnitude and epicentral distance from the earthquakes that triggered associated landslides. Additionally, based on the data from their work, Keefer and Wilson (1989) were able to develop a regression equation to derive the landslide surface as a function of earthquake magnitude. The latter work was updated by Rodriguez et al. (1999) using a larger database, along with some adjustments on correlations, and obtained similar results.

Further attempts to predict earthquake-induced landslides areas were accomplished. To exemplify, Jibson (1993) suggested the use of the Newmark method of landslide modeling, which estimates the displacement as a function of the critical landslide acceleration and seismic shaking intensity. He stated that the suggested method provides significantly more useful information than pseudo-static analysis and is considered to be more practical than finite element modeling. However, finite element approaches are still used due to their simplicity (Islam et al., 2019).

Landslides are complex phenomenon and require the use of numerous surveying tools (e.g., drilling, inclinometer, INSAR, geophysics, global positioning system) to understand their genesis, mechanism, and impacts. Classical geophysical exploration methods (e.g., seismic refraction, electrical resistivity tomography), which are non-destructive, are widely used in slope stability studies (Jongmans and Garambois 2007; Pazzi et al. 2019), to enable a relatively correct characterization of unstable zone geometry (depth and lateral extension). Nevertheless, these methods are expensive and time consuming making their implementation difficult, especially in rugged areas. These limitations can be overcome by relying on the horizontal to vertical spectral ratio (HVSr) method of ambient noise, which is simple, inexpensive, and rapidly implemented than previously mentioned methods. This technique has previously been applied in Algeria as well as worldwide, to identify unstable areas based on spectral response analysis (Hellel et al. 2013). Meziani et al. (2017) pinpointed that the combination of HVSr and geotechnical data allows the identification of landslide geometry.

This work discusses local landslide phenomena in the Mila region based on field observations and noise measurement data collected 3 days after the earthquake in the affected area and their interpretation. The aims are: (a) a better understanding of the landslide predisposing and triggering factors in El Kherba city, (b) identification and characterization of the August 7, 2020 landslide using the HVSr of the ambient noise measurements, and (c) validation of the

obtained results with geological and geotechnical data and field observations.

## Geological and geotechnical setting of the study area

North-eastern Algeria is part of the Maghrebides mountain chain that forms the western Mediterranean belt. This chain is derived from three paleogeographic domains that extend from North to South: the internal domain, the flysch domain, and the external domain.

The study area is located in the Mila basin part of the external domain of the North Eastern Algeria Alpine chain. It is a vast depression of approximately 40 km wide and 120 km long, filled with Neogenic deposits, which overlay a substratum, formed of flysch thrust sheets formations that are generally allochthonous (Coiffait 1992). The geological formations in the Mila region, are represented by a Mesozoic: Triassic evaporites, Jurassic carbonate formations (Durand-Delga 1955), Cretaceous marls, and marly limestones underlying Paleocene–Eocene black marls (Fig. 1). The Miocene and Pliocene formations are predominately characterized by detrital and evaporitic deposits. These deposits show significant spatial extent and are mainly composed of clay or marl. Sandstones, lacustrine limestones, gypsiferous marls, and conglomerates are also present (Coiffait 1992). These Neogene formations display the following characteristics:

- Lacustrine limestone between 50 and 100 m thick in some places (Durand-Delga 1955) with an infiltration potential that allows the soil to be saturated by water, which favors steep slope destabilization.
- Poor lithological and geotechnical characteristics (low shear strength and cohesion) of clay and marl formations, constitute predominant and predisposing factors including a shrinkage-swelling phenomenon (Athmania et al. 2010). These characteristics increase the region's vulnerability to landslide hazard. Quaternary deposits are also present in the valleys, represented by gravels and silty sandstone.

The preliminary results of an unpublished report of in situ and laboratory tests conducted by the National Laboratory for Housing and Construction (LNHC) for the entire Mila region, allowed the identification of two geotechnical units: a clay formation overlying marl bedrock (Zouaoui 2008) (Fig. 2a). The clay formation is sometimes described as silty or sandy for the first two meters, within which gypsum inclusions are found, and its thickness varies from 20 to 38 m. The upper most subsurface unit is characterized by shear velocities of about 100 m/s for depths ranging from 0 to 10 m and 170 m/s beyond 10 m. While density values

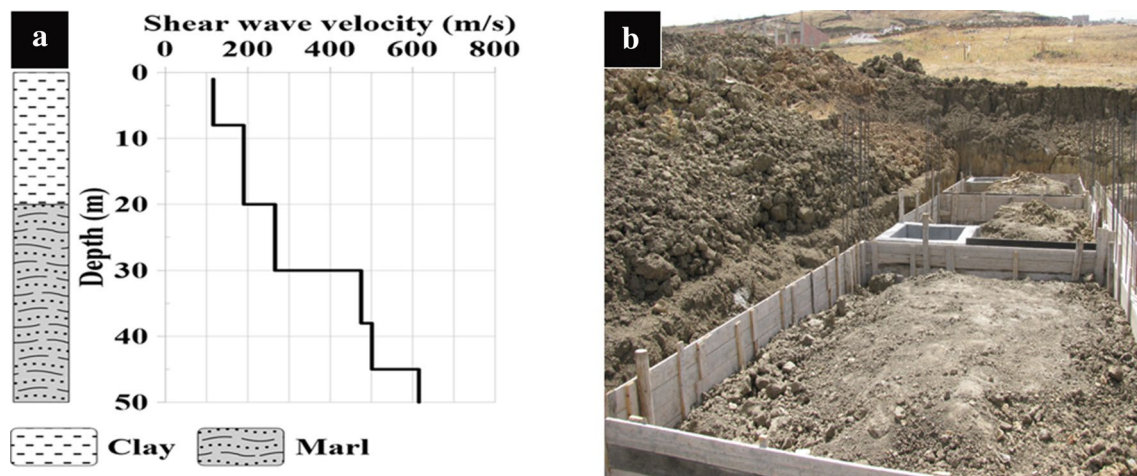


**Fig. 2** a Geotechnical model showing the variation of the shear wave velocity as a function of depth in the two lithological units, b photo taken in the landslide body, showing the anchoring of a new construction in the remoulded part of the clay layer

range from 1.5 to 1.7 ( $\text{KN/m}^3$ ), a water saturation higher than 87% and a plasticity index (PI) ranging from 35 to 40%. These geotechnical parameters indicate a low-density plastic soil, with a high water saturation percentage and swelling potential. The marl formation, situated at an average depth of 30 m, is considered in the current work as geotechnical bedrock since it has a shear velocity varying from 500 to 615 m/s, and a dry density between 1.93 and 2.1 ( $\text{KN/m}^3$ ). The latter formation is marked by a medium to low plasticity with PI ranging from 5 to 10%.

## El Kherba landslide

### Analysis of geological field data

El Kherba city is located about 2 km southwest of Mila city, at an average altitude of 620 m, on sloping terrain with an average angle of  $14^\circ$  dipping toward the north. The built environment is constructed on top of silty clay soil (Fig. 2b). Two main typologies of buildings visibly dominate the locality. First, the traditional one-story houses built of local cut sandstone. Second, recent buildings made of concrete with more than one floor. According to an interview done with residents, most of the buildings are anchored at a depth not exceeding 2 m, meaning they are founded in the clay formation.

No effects (cracks or other damage) were reported directly after the earthquake. Nevertheless, it was only a few hours after the main shock that the cracks started to develop and propagate, resulting in toppled houses. Indeed, in all surveyed sites, the buildings were suffering from structural damage of varying degrees (Fig. 3a, b), resulting in a total collapse even the more recently built houses. Fortunately,

no casualties were reported. The landslide also caused road subsidence in some parts of the locality (Fig. 3c) and the failure of the sewer network (Fig. 3d). Plus, it caused serious damages to crucial structures like a water tower (Fig. 3e) located at the landslide's crown (Fig. 4a).

In addition to the damage caused to the buildings, the landslide caused significant cracks on the ground surface along more than 2 km. Directional rose diagram developed based on field data indicates two predominant trends (Fig. 4b). Most of the observed cracks in the ground surface of the landslide body have trend directions of mainly N55 and N75. Also, less frequent trends in the directions of N25, N135, N165, and N10 were reported. In the field, the N55 and N75 directions are obvious and dominate the other trends and generally can be defined as parallel 'en-echelon' cracks (Fig. 5a). These cracks are located in the upstream part of the landslide, with maximum lengths of 20 m and openings with a width varying between 10 and 20 cm and up to 80 cm deep. Additionally, the cracks do not manifest any vertical throw, as they are located on a low slope and tend to be horizontal.

Further down, the main trends (i.e., N55 and N75) show significant fissures with lengths up to 200 m (Fig. 5b). They are observed continuously from uphill to downhill and are perpendicular to the main landslide direction (South to North). Also, they vary in width and depth of openings from few centimeters to few meters (Fig. 5c, d). The N25 and N135 directions mainly exist in the middle part of the landslide, as well as near its flanks. These cracks have a length of few meters, with openings ranging from few centimeters to few meters and few centimeters deep. The cracks of the N10 and N165 directions characterize the landslide flanks and tend to be parallel to them. Moreover, cracks of these trends are longer relative to the others. Some of these

**Fig. 3** Photos **a, b** show the damage caused by the landslide to the structural elements of the houses, **c** Subsidence and horizontal displacement of a road, **d** Rupture of a sewer pipe, **e** cracks in the water tower and increase of the opening at the rupture joint



cracks reached several hundred meters, with openings in upheaval zone form, reaching 6 m in width in some places. This is well illustrated in the eastern flank where a recently built house collapsed due to the development of such cracks, while at the western flank, there is a road that has undergone a vertical displacement of 2 m. A significant bulge of highly deformed material (accumulation zone) was created at the landslide foothill, as a result of the thrust exerted by sedimentary deposits. This corresponds to an upheaval zone (Fig. 5e, f) where cracks disseminated in all directions.

At the foot of the landslide, pronounced damage is clearly observed where buildings were tilted, torsioned, overturned, and in some instances totally destroyed (Fig. 5g, h).

The spatio-temporal evolution of the landslide is well characterized by the development of landslide-related structures and cracks. Indeed, the buildings have undergone continuous deformation. At the western lateral limit, after the earthquake, the same day, a crack with a centimetric vertical throw appeared on the road pavement where two blocks were lifted and affected a house door

**Fig. 4 a** A view of El Kherba landslide area displaying the investigated sites, Noise measurements and field data (google earth image taken before the event). Ambient noise measurements are shown in colored circles, triangle and square. The square with blue outline indicates the water tower position at the landslide crown. The red arrows indicate the direction of the landslide. The brown stars represent each point's elevation (m). The black arrows point to the direction of the cracks in the field from which the red dotted landslide boundary was established. The orange line shows the AB profile with the name of each point highlighted in yellow. **b** Directional rose diagram showing that most of cracks trend N75°

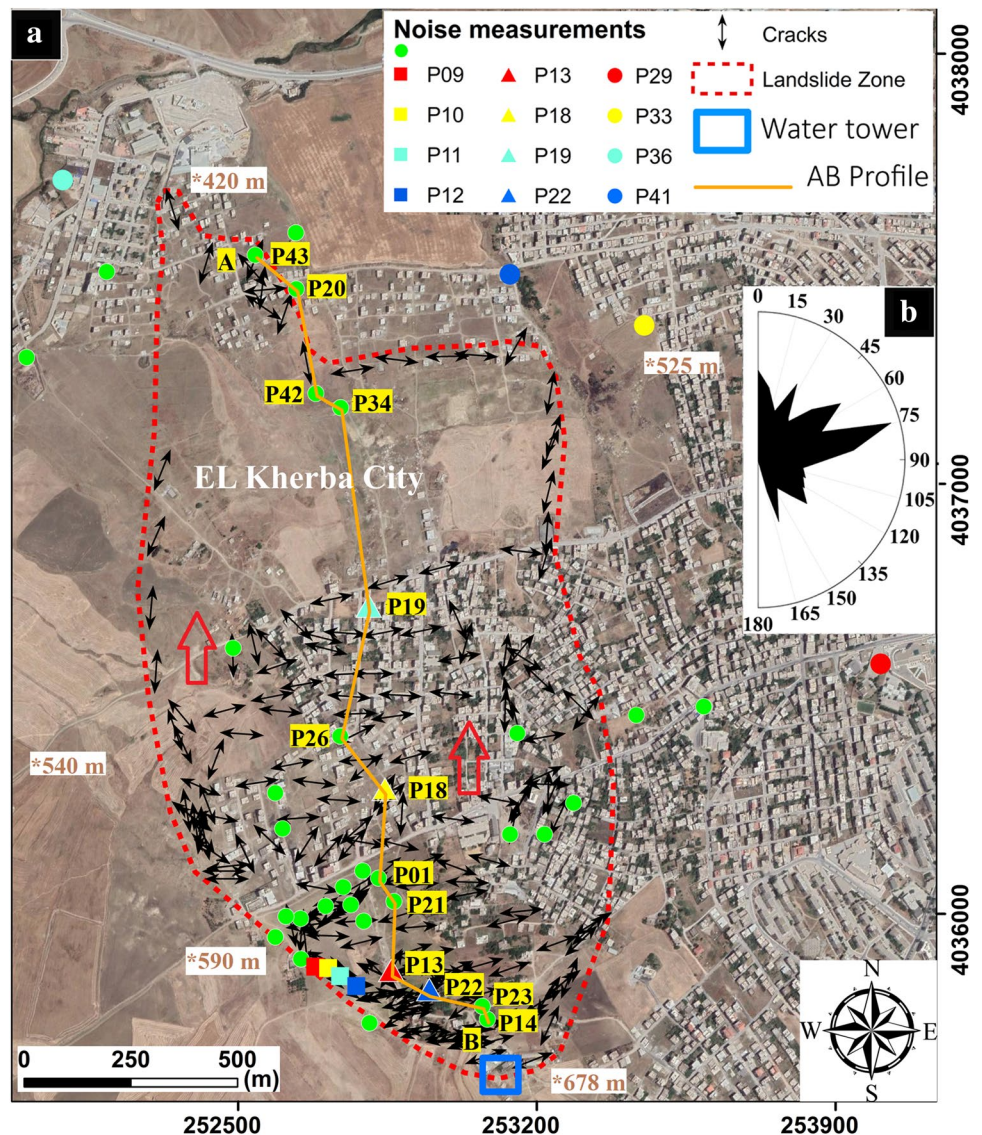


(Fig. 6a). The next day (August 8, 2020) the vertical displacement increased, the eastern compartment of the road pavement had settled and the two blocks were caught in the fissure (Fig. 6b), the eastern part of the door was tilted. On August 9, 2020 the vertical throw reached 1 m and the entire door was tilted northward (Fig. 6c). On August 11, 2020, the door collapsed and was buried in the ground (Fig. 6d). On that day, the vertical throw exceeded 2 m (Fig. 6e).

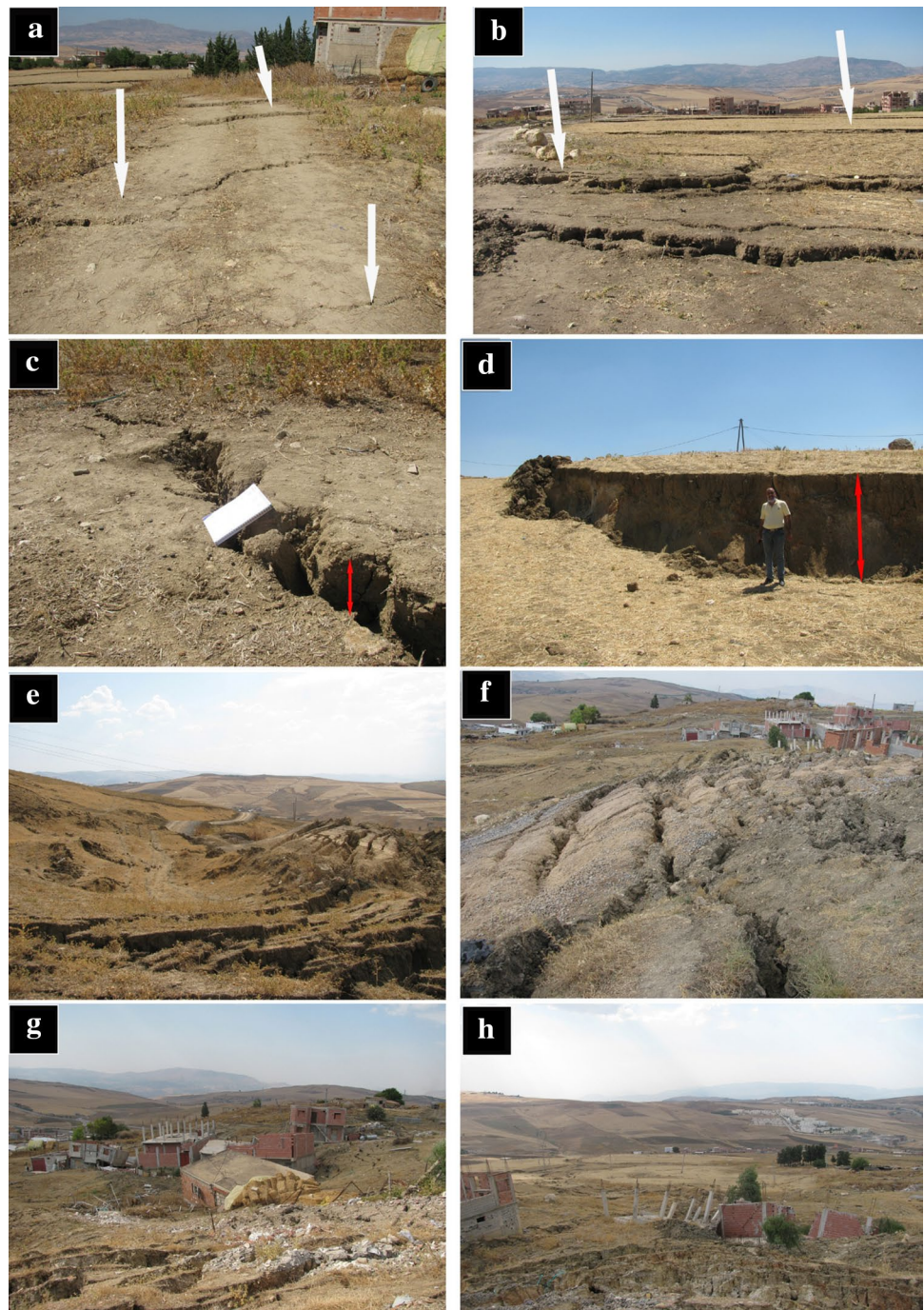
At the eastern flank of the landslide, further evidence illustrating the landslide evolution exists such as a crack that appeared in the pavement without affecting the surrounding building (Fig. 7a). The day after the earthquake, this building tilted northward, the first floor collapsed, and the second floor began to sink into the ground (Fig. 7b). On August 12, 2020, the first floor collapsed completely, and only the second, third, and fourth floors remained visible (Fig. 7c, d).

From the morphological point of view, the total runout length of the landslide is 2.2 km and 1 km wide. The landslide perimeter and area are 5.5 km and 1.6 km<sup>2</sup>, respectively. For this area, the percentage of natural coverage is 77.5% covering more than three thirds of the landslide area with respect to the anthropized one with 22.5%. The vertical drop from the landslide crown ( $H=678$  m) to the most distal point of the landslide toe ( $H=420$  m) is equal to 258 m. This results in a slope angle of 6.6° corresponding to 14.86% slope percentage.

### Ambient noise method and data acquisition

The ambient noise method was first introduced by Kanai (1957) to evaluate a site seismic response of a soft soil overlying rigid to rocky soil. Later, the HVSR method was proposed by Nogoshi (1971) and spread worldwide

**Fig. 5** Examples of fissures (white arrows) and scarps (red arrows) observed in the El Kherba locality: **a** An “en echelon” disposed fissures, **b** a long metric fissures that mark the landslide crown, **c**, **d** scarps with centimetric to metric vertical displacement, photos **e**, **f** taken in the foothill of the landslide showing the beading which is marked by an intense deformation, photos **g**, **h** showing the severity of the damage in the upheaval zone with houses that have undergone an inclination and torsions



by Nakamura (1989). This method evaluates the ground's fundamental resonance frequency using the ambient noise where data is recorded. It involves calculating the spectral ratios of the horizontal and vertical components from the noise recordings using a single sensor (Nakamura 1989), or a sensor network, to determine the shear wave velocity stratification.

Due to the simplicity and rapid implementation of the HVSR, the method has been widely used in site effects and seismic microzonation studies (Fäh et al. 1997; Layadi

et al. 2016; Gosar 2017). Notably, it is extensively used in geological studies such as the mapping of geological layers (Filed and Jacob 1993; Parolai et al. 2002; Tebbouche et al. 2017; Tebbouche and Ait Benamar 2021), soil characterization (Stephenson et al. 2009; Layadi et al. 2018; Panzera et al. 2019), soil structure interaction (Pazzi et al. 2016), and sedimentary basin imaging (Ibs-von Seht and Wohlenberg 1999; Hinzen et al. 2004; D'Amico et al. 2008; Issaadi et al. 2021). It has also been used for other subjects such as buried structure studies (Moisidi et al.

**Fig. 6** Evolution of a lateral scarp from a centimetric **a** to a metric **e** vertical displacement affecting an entrance gate that tipped and then was buried in the ground



2012; Galli et al. 2013; Panzera et al. 2014; Tebbouche et al. 2017).

Moreover, the method is applied for the definition and characterization of landslides (Burjánek et al. 2010, 2012; Pilz et al. 2013; Pazzi et al. 2017; Ma et al. 2019; Hus-sain et al. 2019; Iannucci et al. 2020; Del Gaudio et al. 2008; Panzera et al. 2012) where the different spectral responses are attributed to different landslide zones (stable and unstable). Ma et al. (2019), based on HVSR curves, have demonstrated that each landslide zone is marked by its own response pattern. Indeed, unstable areas are characterized by horizontal polarization (Kolesnikov et al. 2003), where ground motion can be amplified in a direction marked by maximum peak (Pilz et al. 2013). This directivity

is influenced by geological and topographical factors that polarize the ground motion in one main direction. In these cases, to identify the response directivity of the site if it exists, the polarization is analyzed (Burjánek et al. 2010; Del Gaudio et al. 2008; Panzera et al. 2012). It is clear that the ambient noise polarization is parallel to the sliding direction, which is perpendicular to the observed fractures which is not always the case. Indeed, Panzera et al. (2012) highlighted that the polarization angle may be parallel to the aperture cracks due to the main sliding direction that affects the polarization direction. However, the results obtained in the current work show the capability and efficiency of the HVSR method to analyze and identify directivity phenomena in the site response, especially in the presence of unstable slope.



**Fig. 7** Example illustrating landslide evolution showing the tilting and sinking of a building



Three days after the landslide was triggered, ambient noise recording was set up using a City Shark Ambient Vibration Recorder (Chatelain et al. 2012), equipped with a three-component seismometer (Lenartz 5 s) which have a reliable response in (0.2–50 Hz) frequency range. The micro-tremor survey was conducted in the eastern part of El Kherba city, where landslide evidences are apparent. The data acquisition was mainly done in the upper most displaced materials (landslide) on the boundaries, and outside the landslide zone on top of the stable part. This distribution was based on field observations to identify different areas according to their spectral response. Following Sesame guidelines (SESAME 2004), the acquisition time series was set at 20 min with a sampling rate of 200 Hz. Then, the open-source Geopsy software (<http://www.geopsy.org>) was used to estimate the horizontal to vertical spectral ratios, involving the following processing steps:

1. The noise signals were divided into 25 s time windows to which an STA/LTA anti-triggering filter was applied. The latter consists of comparing short- and long-term averages (STA, LTA) allowing the detection and elimination of transient windows. Thus, only stable windows with a uniform noise ratio were selected. According to common assumptions, the window length was set to include at least ten cycles of the lowest analyzed frequency.
2. Spectra are computed for each (Ni) window, where the time signals are transformed into Fourier spectra using the fast Fourier transform (FFT) method at 5% cosine-tapered windows. This apodization process improves the signal properties in the frequency domain.
3. Spectral amplitudes smoothing for each (Ni) window using the Kono and Ohmachi window (Konno and Ohmachi 1998) fixing the smoothing degree parameter ( $b$ ) to 40.

4. Computation of root mean square (RMS) of the smoothed horizontal spectra  $S_h(N_i)$  (1) for each ( $i$ ) window

with  $S_n(N_i)$  North–South component spectrum, and  $S_e(N_i)$  East–West component spectrum;

$$S_h(N_i) = \sqrt{\frac{S_n(N_i)^2 + S_e(N_i)^2}{2}} \tag{1}$$

5.  $H/V$  spectral ratio computation (2) for each ( $N_i$ ) window:

$$\frac{H}{V}(N_i) = \frac{S_h(N_i)}{S_v(N_i)} \tag{2}$$

6. Geometric mean computation (3) of the  $H/V$  spectral ratio for all windows:

$$\frac{H}{V} = 10^{\frac{\sum \log_{10}(\frac{H}{V}(N_i))}{N_i}} \tag{3}$$

7.  $H/V$  curves plot with a standard deviation in both frequency and amplitude.

### Results

The HVSR curves obtained, over a frequency range from 0.5 to 20 Hz, show three distinct patterns. The HVSR curves in the stable part (sites P29, P33, P36, and P41) reveal peaks around 1–1.5 Hz that can be associated with the interface separating the marl and clay layers (Fig. 8).

The sites located on the landslide boundary (Fig. 8) (sites P09, P10, P11, and P12) present a distinct peak in low frequencies, from 0.6 to 0.8 Hz, marked by large amplitudes. Other peaks are also visible in the high frequencies, at about 5, 10 and 14 Hz, but with lower amplitude than those observed previously. Since these peaks are

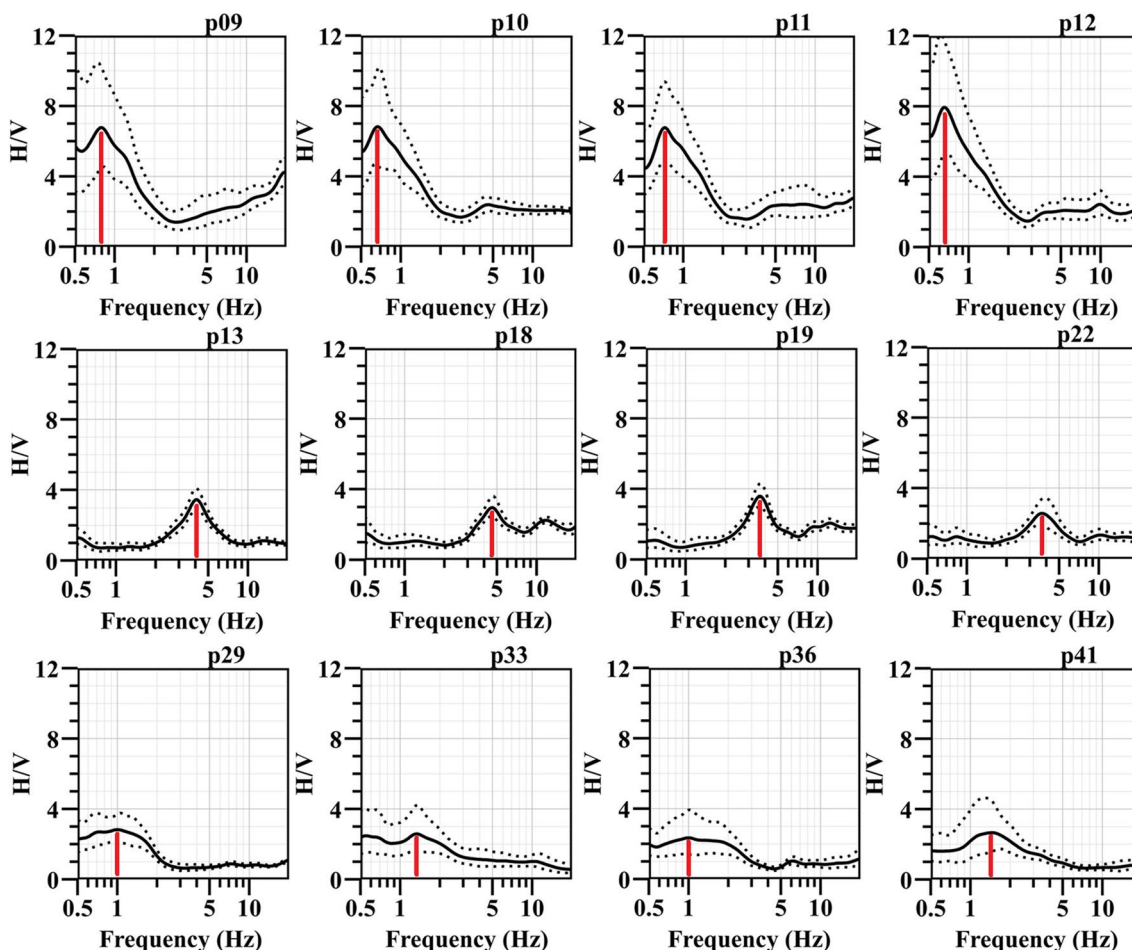


**Fig. 8** HVSR curves obtained from an average of the horizontal components as a function of frequency (Black solid lines) at recording sites located in the landslide limit (first row) unstable zone (second

row) and stable zone (third row). The red line shows the main frequency of each frequency spectra

not visible on the stable part, this suggests the possibility that they may be associated with the presence of fractures at the landslide boundary and near the lateral scarps.

In the unstable part, the HVSR curves (Fig. 8) (sites P13, P18, P19, and P22) display a different pattern from the stable part, but similar to that near the landslide flanks, with entirely different features in high frequencies. Indeed, a very high amplitude peak appears at a frequency between 3 and 14 Hz. The interpretation of this observation, based on local geology, indicate that this peak is typical in the unstable part only, and may be associated solely with the soil remoulding. Indeed, the outcropping clay layer is excessively fractured and reveals an important decrease in its mechanical properties such as density and shear velocity. This could happen due to the mobilization of loosened materials (Kakhki et al. 2020), leading to a low-velocity contrast between the remoulded soil in the upper part and the undisturbed deep part below the surface of the rupture.

Along the AB profile (Fig. 4b), a 2-D profile (Fig. 9a) is obtained from the combination of all the HVSR spectra (Fig. 9b). The latter shows the spectral response over the entire slope, where an amplitude variation can be detected, suggesting that the fracture surface shape has changed. Subsequently, the average shear wave velocity obtained from the LNHC report coupled with the fundamental frequencies derived from HVSR curves enabled the

estimation of the sliding surface depth using Eqs. (4) and (5) (Haskell 1960; Madera 1970):

$$f_0 = \frac{V_s}{4h}, \tag{4}$$

$$V_D = \frac{\sum_{i=1}^n h_i V_{s_i}}{\sum_{i=1}^n h_i} \text{ with } H = \sum_i h_i. \tag{5}$$

Based on the estimated depths, surface of rupture is mapped accurately along AB profile (Fig. 9c). The rupture surface may be located in the shallow clay layer at  $2.14 \pm 0.11$  m to  $8.35 \pm 2.68$  m (see Table 1). The depth variation is reflected by a significant shift in peak's frequency, associated with the landslide thickness decrease, and change in mechanical characteristics and soil properties induced by the landslide (Kakhki et al. 2020). Furthermore, water content plays an important role in triggering landslides. Indeed, a soil's water content above a certain threshold may reduce or diminish cohesion between the grains, which further leads to soil embrittlement.

It is well known that, during precipitation, water soaks the soil, causing changes in its physical parameters and behavior by increasing the pore pressure. As a result, the soil's bearing capacity and resistance decrease. In his analysis of the climatological balance over a period of 20 years (1986–2006),

**Fig. 9** a 2-D diagram obtained from the combination of all the noise measurements along the profile A–B as a function of distance and frequency. b HVSR curves at the recording sites located along the A–B profile in (Fig. 4b). c Geological cross-section along the A–B profile showing the estimated slip surface in red dashed lines

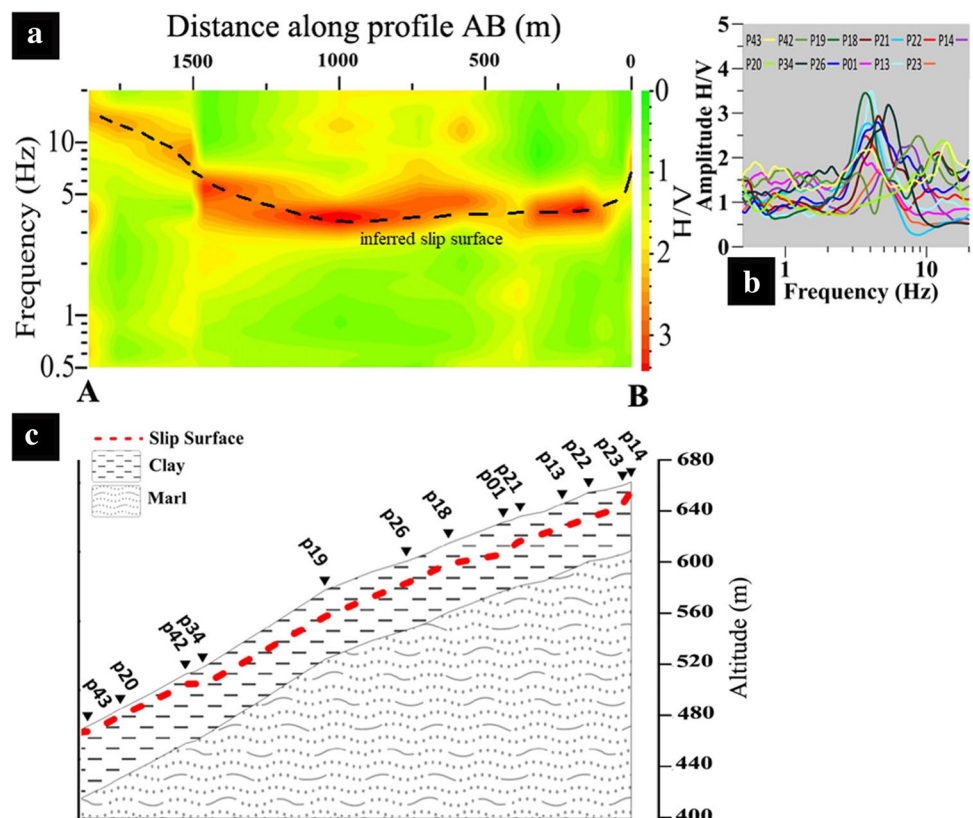


**Table 1** Surface of rupture depth ( $H_{rs}$ ) estimation from combining shear wave velocity from geotechnical model (Fig. 2) and soil frequency  $f_0$  from HVSR curves, using Eqs. (4) and (5)

HVSR sites	HVSR $f_0$ (Hz)	Estimated $H_{rs}$ (m)
p14	$7.25 \pm 0.85$	$4 \pm 0.48$
p23	$4.68 \pm 0.47$	$6.19 \pm 0.63$
p22	$3.72 \pm 0.44$	$7.79 \pm 1.49$
p13	$4.14 \pm 0.27$	$7 \pm 0.46$
p21	$3.89 \pm 0.45$	$7.45 \pm 1.19$
p01	$3.47 \pm 0.61$	$8.35 \pm 2.68$
p18	$4.62 \pm 0.4$	$6.27 \pm 0.55$
p26	$4.34 \pm 0.6$	$6.68 \pm 0.94$
p19	$3.72 \pm 0.24$	$7.79 \pm 0.51$
p34	$5.26 \pm 0.46$	$5.51 \pm 0.49$
p42	$8.87 \pm 1.23$	$3.27 \pm 0.47$
p20	$12.71 \pm 1$	$2.28 \pm 0.18$
p43	$13.57 \pm 0.7$	$2.14 \pm 0.11$

Zouaoui (2008) revealed that Mila region is characterized by a cold and humid period from November to May, and a hot and dry period from June to September. This highlights the absence of a concomitance of rainfalls that might have contributed to the landslide.

In our case, the water table depth measured on August 12, 2020 in a well located at the unstable part was 2 m. In addition, a significant amount of water was released due to leakage from a water tower located above the landslide crown (Fig. 4a), which soaked into the ground for more than 6 months. This suggests that the water content in the shallow soil reached a very high level leading to an increase in P-wave velocities and  $H/V$  ratio. This phenomenon may be one of the reasons for the high peak values observed in the unstable zone.

In particular, the ambient noise data was used in the analysis of the site response directivity by rotating the horizontal components of the spectral ratios obtained at each measurement point in 10 degree steps from  $0^\circ$  to  $180^\circ$ . The results of the directional variation of these HVSR ratios are shown in Fig. 10. The resulting directivity pattern of ambient noise is quite complex and shows strong variations between the different areas. In the stable part (Fig. 10a), where the HVSR curves indicate peaks in the low frequencies as shown above, the HVSR rotation does not show any preferential direction over the whole frequency range. Based on field observations, this part shows no cracks or deformation. This can indicate that the directivity could be controlled by the fracture system.

In the unstable part (Fig. 10b), the rotated spectral ratios indicate clear directional effects in the high frequencies, with an angle of about  $145^\circ$  at the P13 and P18 sites. Moving northward, at the P19 and P34 sites, the directions are

about  $10^\circ$  and  $25^\circ$ , respectively. The obtained directivity values are the same at the P13 and P18 sites, located on the displaced part of the landslide where the cracks are dense and their dominant direction tends towards  $55^\circ$ – $75^\circ$  which is perpendicular to the  $H/V$  rotate direction. Such results correspond perfectly to that demonstrated by Burj'aneq et al. (2010), showing that the directivity of the ambient noise is perpendicular to the observed fractures and parallel to the landslide direction.

Sites P19 and P34 are located in less fissured parcels with shallow heterogeneities caused by the thrust of the crown's material moving by gravitational force. Thus, both sites have different directions even if they are in the same zone. However, the P13 and P18 sites in the upper part of the landslide, have a similar angle of directivity. Moreover, the spectral response in this part shows frequencies corresponding to deeper contrasts than those observed in the northern part of the landslide. Therefore, the high frequencies variation (shift) might be controlled by two factors: (a) the shallow heterogeneities and (b) the fact that each portion of the sliding part vibrates separately at different frequencies and directions. This explanation is in line with that already advanced by Pilz et al. (2013).

Away from the unstable part, on the landslide limit (Fig. 10c), clear directional effects are present in low frequencies while the directional resonance angle changes, which makes their interpretation quite complex compared to the other two parts. We notice that there is no prevailing direction and the amplitude decreases at high frequencies where peaks associated with the rupture surface were observed. Therefore, these results are due to the increasing rock stiffness in this part.

## Discussion and conclusion

Landslides triggered by an earthquake remain a pressing issue, considering their complexity and the potential for significant human and economic impacts. Their characterization is a particular challenge for engineers, especially in urban areas. This work outlines a post-impact field study of El Kherba landslide triggered by the Mila earthquake of August 7, 2020. The aim is to characterize this event using a combination of geological and geophysical data, as well as field observations.

The analysis of the data collected and field observations enabled the identification of three crack directions. The N55 and N75 directions mark the major escarpments up to 200 m long and perpendicular to the main direction of the landslide, which is the most dominant direction. The N25 and N135 directions characterize the core of the landslide and its lateral boundaries. Along these boundaries, there is another

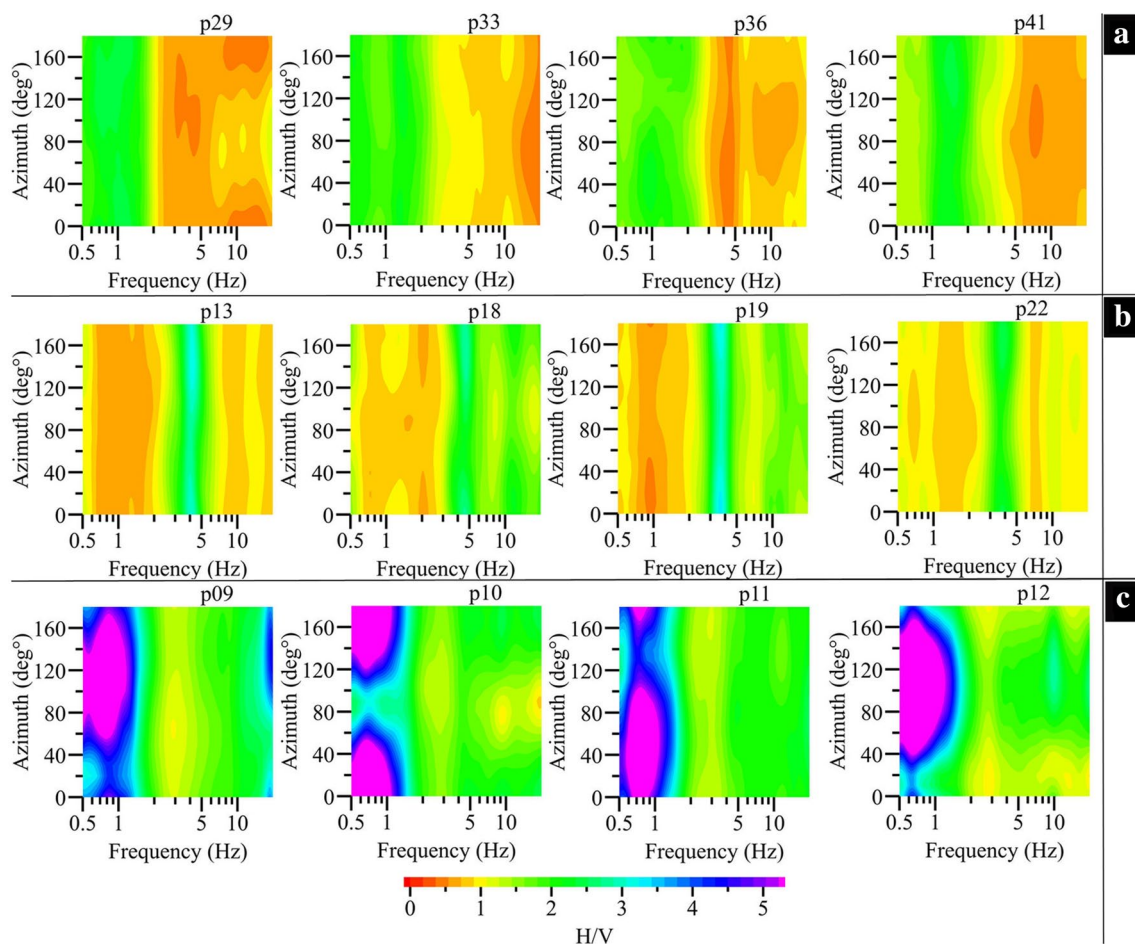


**Fig. 10** Azimuthal variations of HVSR values obtained at selected ambient noise recording sites

class of direction, N110 and N165, marked by the largest openings reaching up to 6 m in width.

This crack network affected the outcropping clay layer throughout the locality. This formation, with weak geotechnical characteristics at shallow depths (see geological and geotechnical setting), combined with a 15% slope, was already prone to landslides, especially since the water table is at 2 m deep. Moreover, due to the earthquake impact the water tower located above the landslide body experienced heavy damage (Fig. 3e). The tower was ultimately emptied to avoid its total destruction. The water soaking into the underlying soil increased the site's vulnerability to landslides by increasing the pore pressure, which tends to eliminate soil rigidity.

In this work, the field investigation data were incorporated with the experimental one, i.e., the HVSR method ambient noise that was used throughout the area. The notable feature of this work is the dense measurement points that were carried out immediately after the landslide was triggered, prior to any other type of investigation, on a landslide that was still active. The results of the HVSR revealed

that the fundamental resonance properties of an earthquake-induced landslide, based on ambient noise recordings, can be obtained with a limited number of stations and an acquisition time of a few hours. Regarding the curves typology, the use of ambient noise measurements allowed the identification of three distinct zones: (1) a stable zone, where the curves display a low-amplitude dominant peak at about 1–1.5 Hz, related to a lithological contrast; (2) an unstable zone, characterized by a high frequency peak not observed on the stable zone, related both to soil remoulding, as well as to the increase of water content, which point to the presence of an active slip surface inside the clay layer; and (3) a third zone at the boundary of the landslide, which marks the transition between the stable zone and the unstable zone. The latter part is marked by a low-frequency peak with a very pronounced amplitude, confirming that heterogeneities and changes recognized using HVSR ambient noise are due to the landslide's movements.

Despite the lack of detailed information on the physical parameters of the soil, the depth of the fracture surface was estimated by empirical equations using the HVSR ambient

noise, demonstrating the potential of this method in mapping geological evidence on unstable slopes. HV measures can give accurate results, especially in homogeneous geological units, but their reliability is tied to soil physical parameters such as shearing velocity and depth H.

The HVSR measurements were also performed to analyze the directivity response of the landslide body. The obtained results match the field observations and the H/V spectral ratios. The stable part shows no directivity effect, while the unstable and margin areas have their own directivity response, which indicates that the directivity is controlled by the cracks network and soil remoulding. The observed change in directivity response in the unstable part, and at the landslide boundary, suggests that directional amplification may not be directly related to the slope direction of a landslide and that it is controlled by several factors that are difficult to identify.

The results obtained after combining field data with ambient noise HVSR can provide insights into earthquake-induced landslide studies. The causal factors were first examined through observations and analysis of the ambient noise, which contributed to a better understanding of the phenomenon that occurred. They were also used for rapid geometric identification, even if the results obtained are sometimes difficult to interpret. This demonstrates the effectiveness of the HVSR ambient noise method in the study of active landslides where the unstable mass, composed of remoulded soil, overlay a compact basement. Moreover, by its rapid implementation, the use of the HVSR method immediately after this type of event enables an initial appreciation of the unstable area extent, and may even guide future recognition campaigns. It is also worth stating that the same technique can be used elsewhere in northern Algeria, where identical geomorphological and geological features prevail.

The characterization of the different landslide parts and its geometry in this study could be a useful tool for planners involved in decision making related to the redevelopment of El Kherba city, as well as in site studies for future constructions.

**Acknowledgements** This work is supported by the CGS (Centre National de Recherche Appliquée en Génie Parasismique, Algiers). We thank everyone provided assistance in the process of conducting this research. We are deeply indebted to the civil authorities, local inhabitants of El Kherba and Nourredine Mezouar for their important help in the field. The authors are grateful to the editor as well as Vincenzo Del Gaudio and the anonymous reviewer for their useful suggestions and constructive comments that improved the quality of the manuscript.

**Funding** This research did not receive any specific grant from funding agencies in the public, commercial, or not-for-profit sectors.

## Declarations

**Conflicts of interest** The authors declare no conflict of interest.

**Authorship statement** All authors certify that they have participated sufficiently in this work. Furthermore, each author certifies that this material or similar material has not been and will not be submitted to or published in any other publication before its appearance in the Environmental Earth Sciences Journal.

## References

- Athmania D, Benaissa A, Hammadi A, Bouassida M (2010) Clay and marl formation susceptibility in Mila Province. Algeria Geotech Geol Eng 28(6):805–813. <https://doi.org/10.1007/s10706-010-9341-5>
- Benfedda A, Bouhadad Y, Boughacha MS, Guessoum N, Abbas K, Bezzeghoud M (2020) The Oran January 9th ( $M_w$  4.7) and June 6th, 2008 ( $M_w$  5.4) earthquakes: seismological study and seismotectonic implication. J Afr Earth Sci. <https://doi.org/10.1016/j.jafrearsci.2020.103896>
- Burjánek J, Gassner-Stamm G, Poggi V, Moore JR, Fäh D (2010) Ambient vibration analysis of an unstable mountain slope. Geophys J Int 180(2):820–828. <https://doi.org/10.1111/j.1365-246X.2009.04451.x>
- Burjánek J, Moore JR, Yugsi Molina FX, Fäh D (2012) Instrumental evidence of normal mode rock slope vibration. Geophys J Int 188(2):559–569. <https://doi.org/10.1111/j.1365-246X.2011.05272.x>
- Chatelain JL, Guillier B, Gueguen P, Fréchet J, Sarraut J (2012) Ambient vibration recording for single-station, array and building studies made simple: CityShark II. Int J Geosci 3:1168–1175. <https://doi.org/10.4236/ijg.2012.326118>
- Chousianitis K, Del Gaudio V, Kalogeras I, Ganas A (2014) Predictive model of Arias intensity and Newmark displacement for regional scale evaluation of earthquake-induced landslide hazard in Greece. Soil Dyn Earthq Eng 65:11–29. <https://doi.org/10.1016/j.soildyn.2014.05.009>
- Coiffait PE (1992) Un bassin post-nappes dans son cadre structural: l'exemple du bassin de Constantine (Algérie nord-orientale). Ph.D. thesis, Henri Poincaré Nancy I University
- D'Amico V, Picozzi M, Baliva F, Albarello D (2008) Ambient noise measurements for preliminary site-effects characterization in the urban area of Florence, Italy. Bull Seismol Soc Am 98(3):1373–1388. <https://doi.org/10.1785/0120070231>
- Del Gaudio V, Coccia S WJ, Gallipoli MR, Mucciarelli M (2008) Detection of directivity in seismic site response from microtremor spectral analysis. Nat Hazard 8(4):751–762
- Delgado J, Peláez JA, Tomás R, García-Tortosa FJ, Alfaro P, Casado CL (2011) Seismically-induced landslides in the Betic Cordillera (S Spain). Soil Dyn Earthq Eng 31(9):1203–1211. <https://doi.org/10.1016/j.soildyn.2011.04.008>
- Durand-Delga M (1955) Etude géologique de l'ouest de la chaîne numidique. Service de la Carte Géologique de l'Algérie 2(29)
- Fäh D, Rüttener E, Noack T, Krusan P (1997) Microzonation of the city of Basel. J Seismolog 1(1):87–102. <https://doi.org/10.1023/A:1009774423900>
- Field E, Jacob K (1993) The theoretical response of sedimentary layers to ambient seismic noise. Geophys Res Lett 20(24):2925–2928. <https://doi.org/10.1029/93GL03054>
- Gabert P (1984) Séismes, néotectonique et effets induits sur les versants des massifs des Babors dans la région de Kerrata (Algérie). Méditerranée 1–2:25–31
- Galli PAC, Giocoli A, Peronace E, Piscitelli S, Quadrio B, Bellanova J (2013) Integrated near surface geophysics across the active Mount Marzano Fault System (southern Italy): seismogenic

- hints. *Int J Earth Sci* 103(1):315–325. <https://doi.org/10.1007/s00531-013-0944-y>
- Gosar A (2017) Study on the applicability of the microtremor HVSR method to support seismic microzonation in the town of Idrija (W Slovenia). *Nat Hazard* 17(6):925. <https://doi.org/10.5194/nhess-17-925-2017>
- Guemache MA, Machane D, Beldjoudi H, Gharbi S, Djadia L, Benahmed S, Ymmel H (2010) On a damaging earthquake-induced landslide in the Algerian Alps: the March 20, 2006 Laâlam landslide (Babors chain, northeast Algeria), triggered by the Kherrata earthquake ( $M_w = 5.3$ ). *Nat Hazards* 54(2):273–288. <https://doi.org/10.1007/s11069-009-9467-z>
- Harbi A, Maouche S, Ayadi A (1999) Neotectonics and associate seismicity in the Eastern Tellian Atlas of Algeria. *J Seismolog* 3(1):95–104. <https://doi.org/10.1023/A:1009743404491>
- Harbi A, Benouar D, Benhallou H (2003) Re-appraisal of seismicity and seismotectonics in the north-eastern Algeria part I: review of historical seismicity. *J Seismol* 7(1):115–136. <https://doi.org/10.1023/A:1021212015935>
- Haskell NA (1960) Crustal reflection of plane SH waves. *J Geophys Res* 65(12):4147–4150. <https://doi.org/10.1029/JZ065i012p04147>
- Hellel M, Chatelain JL, Cheikh-Lounis G, Machane D, Guillier B, Haddoum H (2013) Utilisation de la méthode h/v bruit de fond pour l'estimation rapide de la géométrie d'une zone instable : cas du glissement d'une route à Lakhdaria (Algérie). *Bulletin Du Service Géologique National* 22(1):1–11
- Hinzen KG, Weber B, Scherbaum F (2004) On the resolution of H/V measurements to determine sediment thickness, a case study across a normal fault in the Lower Rhine Embayment, Germany. *J Earthq Eng* 8(06):909–926
- Hussain Y, Cardenas-Soto M, Uagoda R, Martino S, Sanchez NP, Moreira CA, Martinez-Carvajal H (2019) Shear wave velocity estimation by a joint inversion of HVSR and fk curves under diffuse field assumption: a case study of Sobradinho landslide. *Anuário Do Instituto De Geociências* 42(1):742–750. [https://doi.org/10.11137/2019\\_1\\_742\\_750](https://doi.org/10.11137/2019_1_742_750)
- Iannucci R, Martino S, Paciello A, D'Amico S, Galea P (2020) Investigation of cliff instability at GhajnHadid Tower (Selmun Promontory, Malta) by integrated passive seismic techniques. *J Seismol*. <https://doi.org/10.1007/s10950-019-09898-z>
- Ibs-von Seht M, Wohlenberg J (1999) Microtremor measurements used to map thickness of soft sediments. *Bull Seismol Soc Am* 89(1):250–259. <https://doi.org/10.1785/BSSA0890010250>
- Islam N, Hawlader B, Wang C, Soga K (2019) Large-deformation finite-element modelling of earthquake-induced landslides considering strain-softening behaviour of sensitive clay. *Can Geotech J* 56(7):1003–1018. <https://doi.org/10.1139/cgj-2018-0250>
- Issaadi A, Semmane F, Yelles-Chaouche A, Galiana-Merino JJ, Mazari A (2021) Shallow S-wave velocity structure in the Middle-Chelif Basin, Algeria, using ambient vibration single-station and array measurements. *Appl Sci* 11(22):11058. <https://doi.org/10.3390/app112211058>
- Jibson RW (1993) Predicting earthquake-induced landslide displacements using Newmark's sliding block analysis. *Transp Res Rec* 1411:9–17
- Jongmans D, Garambois S (2007) Geophysical investigation of landslides: a review. *Bulletin De La Société Géologique De France* 178(2):101–112. <https://doi.org/10.2113/gssgfbull.178.2.101>
- Kakhki MK, Peters FC, Mansur WJ, SadidKhoii A, Rezaei S (2020) Deciphering site response directivity in landslide-prone slopes from ambient noise spectral analysis. *Eng Geol* 269:105542. <https://doi.org/10.1016/j.enggeo.2020.105542>
- Kanai K (1957) Semi-empirical formula for the seismic characteristics of the ground. *Bull Earthq Res Inst Univ Tokyo* 35(2):309–325
- Keefer DK (1984) Landslides caused by earthquakes. *Geol Soc Am Bull* 95(4):406–421. [https://doi.org/10.1130/0016-7606\(1984\)95<406:LCBE>2.0.CO;2](https://doi.org/10.1130/0016-7606(1984)95<406:LCBE>2.0.CO;2)
- Keefer DK, Wilson RC (1989) Predicting earthquake-induced landslides, with emphasis on arid and semi-arid environments. *Landslides Semi-Arid Environ* 2(1):118–149
- Kolesnikov YI, Nemirovich-Danchenko MM, Goldin SV, Seleznev VS (2003) Slope stability monitoring from microseismic field using polarization methodology. *Nat Hazards Earth Syst Sci* 3(6):515–521. <https://doi.org/10.5194/nhess-3-515-2003>
- Konno K, Ohmachi T (1998) Ground-motion characteristics estimated from spectral ratio between horizontal and vertical components of microtremor. *Bull Seismol Soc Am* 88(1):228–241. <https://doi.org/10.1785/BSSA0880010228>
- Layadi K, Semmane F, Yelles-Chaouche AK (2016) Site-effects investigation in the city of Chlef (Formerly El-Asnam), Algeria, using earthquake and ambient vibration data. *Bull Seismol Soc Am* 106(5):2185–2196. <https://doi.org/10.1785/0120150365>
- Layadi K, Semmane F, Yelles-Chaouche A (2018) S-wave velocity structure of Chlef City, Algeria, by inversion of Rayleigh wave ellipticity. *Near Surf Geophys* 16(3):328–339. <https://doi.org/10.3997/1873-0604.2018011>
- Ma N, Wang G, Kamai T, Doi I, Chigira M (2019) Amplification of seismic response of a large deep-seated landslide in Tokushima, Japan. *Eng Geol* 249:218–234. <https://doi.org/10.1016/j.enggeo.2019.01.002>
- Machane D, Bouhadad Y, Oubaiche EH, Hellel M, Amrouche F (2004) Description morphologique des effets induits par le séisme de Boumerdes (Algérie) du 21 mai 2003 (Mw= 6.8). *Mémoires Du Service Géologique De L'algérie* 12:133–146
- Madera GA (1970) Fundamental period and amplification of peak acceleration in layered systems. MIT Department of Civil Engineering, Inter-American Program
- Marmi R, Kacimi M, Boularak M (2008) Les mouvements de terrain dans la région de Mila (Algérie Nord-Orientale): impact sur les infrastructures. *Revista De Geomorfologie* 10:51–56
- Martino S, Battaglia S, D'Alessandro F, Della Seta M, Esposito C, Martini G, Pallone F, Troiani F (2019) Earthquake-induced landslide scenarios for seismic microzonation: application to the Accumoli area (Rieti, Italy). *Bull Earthq Eng*. <https://doi.org/10.1007/s10518-019-00589-1>
- Merghadi A, Abderrahmane B, Tien Bui D (2018) Landslide susceptibility assessment at Mila Basin (Algeria): a comparative assessment of prediction capability of advanced machine learning methods. *ISPRS Int J Geo Inf* 7(7):268. <https://doi.org/10.3390/ijgi7070268>
- Meziani B, Machane D, Bendaoud A, Lounis GC, Oubaiche EH, Chabane S, Bensalem R, Moulouel H (2017) Geotechnical and geophysical characterization of the Bouira-Algiers Highway (Ain Turk, Algeria) landslide. *Arab J Geosci* 10(5):117. <https://doi.org/10.1007/s12517-017-2926-z>
- Moisidi M, Vallianatos F, Soupios P, Kershaw S (2012) Spatial spectral variations of microtremors and electrical resistivity tomography surveys for fault determination in southwestern Crete, Greece. *J Geophys Eng* 9(3):261–270. <https://doi.org/10.1088/1742-2132/9/3/261>
- Nakamura Y (1989) A method for dynamic characteristics estimation of subsurface using microtremor on the ground surface. *Railw Tech Res Inst Q Rep* 30(1):25–33
- Nogoshi M (1971) On the amplitude characteristics of microtremor, Part II. *J Atmos Ocean Technol* 24:26–40
- Ogila WAM (2021) Analysis and assessment of slope instability along international mountainous road in North Africa. *Nat Hazards* 106(3):2479–2517. <https://doi.org/10.1007/s11069-021-04552-9>
- Ousadou F, Dorbath L, Dorbath C, Bounif MA, Benhallou H (2013) The Constantine (Algeria) seismic sequence of 27 October 1985: a

- new rupture model from aftershock relocation, focal mechanisms, and stress tensors. *J Seismol* 17(2):207–222. <https://doi.org/10.1007/s10950-012-9320-9>
- Panzerà F, D'Amico S, Lotteri A, Galea P, Lombardo G (2012) Seismic site response of unstable steep slope using noise measurements: the case study of Xemxija Bay area, Malta. *Nat Hazards* 12(11):3421. <https://doi.org/10.5194/nhess-12-3421-2012>
- Panzerà F, Pischiutta M, Lombardo G, Monaco C, Rovelli A (2014) Wavefield polarization in fault zones of the western flank of Mt. Etna: observations and fracture orientation modelling. *Pure Appl Geophys* 171(11):3083–3097. <https://doi.org/10.1007/s00024-014-0831-x>
- Panzerà F, Romagnoli G, Tortorici G, D'Amico S, Rizza M, Catalano S (2019) Integrated use of ambient vibrations and geological methods for seismic microzonation. *J Appl Geophys* 170:103820. <https://doi.org/10.1016/j.jappgeo.2019.103820>
- Parolai S, Bormann P, Milkereit C (2002) New relationships between Vs, thickness of sediments, and resonance frequency calculated by the H/V ratio of seismic noise for the Cologne area (Germany). *Bull Seismol Soc Am* 92(6):2521–2527. <https://doi.org/10.1785/0120010248>
- Pazzi V, Morelli S, Fidolini F, Krymi E, Casagli N, Fanti R (2016) Testing cost-effective methodologies for flood and seismic vulnerability assessment in communities of developing countries (Dajç, northern Albania). *Geomat Nat Hazards Risk* 7(3):971–999. <https://doi.org/10.1080/19475705.2015.1004374>
- Pazzi V, Tanteri L, Bilocchi G, D'Ambrosio M, Caselli A, Fanti R (2017) H/V measurements as an effective tool for the reliable detection of landslide slip surfaces: case studies of Castagnola (La Spezia, Italy) and Roccalbegna (Grosseto, Italy). *Phys Chem Earth* 98:136–153. <https://doi.org/10.1016/j.pce.2016.10.014>
- Pazzi V, Morelli S, Fanti R (2019) A review of the advantages and limitations of geophysical investigations in landslide studies. *Int J Geophys*. <https://doi.org/10.1155/2019/2983087>
- Pilz M, Parolai S, Bindi D, Saponaro A, Abdybachev U (2013) Combining seismic noise techniques for landslide characterization. *Pure Appl Geophys* 171(8):1729–1745. <https://doi.org/10.1007/s00024-013-0733-3>
- Rodriguez CE, Bommer JJ, Chandler RJ (1999) Earthquake-induced landslides: 1980–1997. *Soil Dyn Earthq Eng* 18(5):325–346. [https://doi.org/10.1016/S0267-7261\(99\)00012-3](https://doi.org/10.1016/S0267-7261(99)00012-3)
- Sassa K, Fukuoka H, Scarascia-Mugnozza G, Evans S (1996) Earthquake-induced-landslides: distribution, motion and mechanisms. *Soils Found* 36:53–64. [https://doi.org/10.3208/sandf.36.Special\\_53](https://doi.org/10.3208/sandf.36.Special_53)
- Sato HP, Harp EL (2009) Interpretation of earthquake-induced landslides triggered by the 12 May 2008, M7.9 Wenchuan earthquake in the Beichuan area, Sichuan Province, China using satellite imagery and Google Earth. *Landslides* 6(2):153–159. <https://doi.org/10.1007/s10346-009-0147-6>
- Semmane F, Abacha I, Yelles-Chaouche AK, Haned A, Beldjoudi H, Amrani A (2012) The earthquake swarm of December 2007 in the Mila region of northeastern Algeria. *Nat Hazards* 64(2):1855–1871. <https://doi.org/10.1007/s11069-012-0338-7>
- SESAME (2004) Guidelines for the implementation of the H/V spectral ratio technique on ambient vibrations. Measurements, processing and interpretation. European Commission—Research General Directorate Project No. EVG1-CT-2000–00026 SESAME, report D23.12
- Stephenson WJ, Hartzell S, Frankel AD, Asten M, Carver DL, Kim WY (2009) Site characterization for urban seismic hazards in lower Manhattan, New York City, from microtremor array analysis. *Geophys Res Lett*. <https://doi.org/10.1029/2008GL036444>
- Tebbouche MY, Ait Benamar D (2021) Contribution to the site effects analyses: mapping the thickness of sediments in the Mitidja basin (Algeria) using ambient noise. *Algérie Equip* 64:60–70
- Tebbouche MY, Machane D, Chabane S, Oubaiche EH, Meziani AA, Ait-Benamar D, Moulouel H, Cheikh-Lounis G, Bensalem R, Bendaoud A (2017) Imagery of the metamorphic bedrock roof of the Sahel active fault in the Sablettes (Algiers) reclaimed area by ambient vibration HVSR. *Arab J Geosci* 10(13):292. <https://doi.org/10.1007/s12517-017-3074-1>
- Yelles-Chaouche A, Boudiaf A, Djellit H, Bracene R (2006) La tectonique active de la région nord-algérienne. *CR Geosci* 338(1–2):126–139. <https://doi.org/10.1016/j.crte.2005.11.002>
- Zouaoui S (2008) Etude géologique et géotechnique des glissements de terrains dans le bassin néogène de Mila: Glissement de Sibari. Magister thesis, Hadj Lakhdar-Batna University

**Publisher's Note** Springer Nature remains neutral with regard to jurisdictional claims in published maps and institutional affiliations.